AGU ADVANCING EARTH AND SPACE SCIENCE

Geophysical Research Letters®

RESEARCH LETTER
10.1029/2022GL101191

Glacial Isostatic Adjustment Shapes Proglacial Lakes Over Glacial Cycles

J. Austermann[1], A. D. Wickert[2,3,4], T. Pico[5], J. Kingslake[1], K. L. Callaghan[1], and R. C. Creel[1]

[1]Lamont-Doherty Earth Observatory, Columbia University, Palisades, NY, USA, [2]Saint Anthony Falls Laboratory, University of Minnesota, Minneapolis, MN, USA, [3]Department of Earth & Environmental Sciences, University of Minnesota, Minneapolis, MN, USA, [4]GFZ German Research Centre for Geosciences, Potsdam, Germany, [5]Earth & Planetary Sciences, University of California Santa Cruz, Santa Cruz, CA, USA

Key Points:

- We self-consistently model proglacial lakes that form around the Laurentide ice sheet over the last glacial cycle
- Glacial isostatic adjustment increases the volume and lake depth of proglacial lakes during the deglaciation compared to the glaciation
- When the ice margin retreated over areas of low-lying topography, ice retreat was faster in areas that bordered proglacial lakes

Supporting Information:

Supporting Information may be found in the online version of this article.

Correspondence to:

J. Austermann,
jackya@ldeo.columbia.edu

Citation:

Austermann, J., Wickert, A. D., Pico, T., Kingslake, J., Callaghan, K. L., & Creel, R. C. (2022). Glacial isostatic adjustment shapes proglacial lakes over glacial cycles. *Geophysical Research Letters*, *49*, e2022GL101191. https://doi.org/10.1029/2022GL101191

Received 9 SEP 2022
Accepted 21 NOV 2022

Author Contributions:

Conceptualization: J. Austermann, A. D. Wickert, T. Pico
Formal analysis: J. Austermann
Funding acquisition: J. Austermann, A. D. Wickert
Investigation: J. Austermann, A. D. Wickert, T. Pico, J. Kingslake, K. L. Callaghan, R. C. Creel
Methodology: J. Austermann, A. D. Wickert, T. Pico, J. Kingslake, K. L. Callaghan, R. C. Creel
Software: J. Austermann
Visualization: J. Austermann
Writing – original draft: J. Austermann

Abstract As ice sheets load Earth's surface, they produce ice-marginal depressions which, when filled with meltwater, become proglacial lakes. We include self-consistently evolving proglacial lakes in a glacial isostatic adjustment (GIA) model and apply it to the Laurentide ice sheet over the last glacial cycle. We find that the locations of modeled lakes and the timing of their disappearance is consistent with the geological record. Lake loads can deflect topography by >10 m, and volumes collectively approach 30–45 cm global mean sea-level equivalent. GIA increases deglaciation-phase lake volume up to five-fold and average along-ice-margin depth ≤90 m compared to glaciation-phase ice volume analogs—differences driven by changes in the position and size of the peripheral bulge. Since ice-marginal lake depth affects grounding-line outflow, GIA-modulated proglacial lake depths could affect ice-sheet mass loss. Indeed, we find that Laurentide ice-margin retreat rate sometimes correlates with proglacial lake presence, indicating that proglacial lakes aid glacial collapse.

Plain Language Summary The Laurentide ice sheet grew to its greatest extent during the last glacial maximum, covering most of Canada and the northern part of the US. During its existence, lakes formed adjacent to the ice sheet as seasonal melt water filled the topography around its edge. As the ice sheet grew and melted it changed the topography of Earth's surface by warping the ground beneath the ice sheet and around its edges. In this paper we investigate how this topographic change affected lakes around the ice sheet. We find that it caused lakes to be much bigger during the deglaciation, when the ice sheet retreated and left lows in the topography that took thousands of years after the retreat to fully rebound. We also find that these lakes were deeper at the edge of the ice sheet as the ice sheet collapsed than as it grew, which might have caused faster ice sheet collapse since ice sheets lose mass faster if they end in a lake rather than if they end on land. Our finding shows that lakes might play an important role in how fast past ice sheets grew and collapsed.

1. Introduction

Proglacial lakes are freshwater bodies that form within topographic depressions at an ice sheet's terrestrial margin. These depressions can preexist, or they can be established (or enhanced) by the presence of the ice sheet through its ability to dam water directly and to generate isostatic depressions. Proglacial lakes formed at the margins of both the Laurentide and Fennoscandian ice sheets during the Quaternary (Gorlach et al., 2017; M. Lewis et al., 2021; Mangerud et al., 2004; Murton & Murton, 2012; Smith, 1994). While many proglacial lakes were small and temporary, others spanned thousands of square kilometers and lasted thousands of years (Carrivick & Tweed, 2013). At present, the paleo-shorelines of proglacial lakes are often not found at a constant elevation because they have been deformed due to glacial isostatic adjustment (GIA), which is the response of the Earth's topography, gravity field, and rotation axis to changes in ice and ocean loads (e.g., M. Lewis et al., 2021). Shoreline deformation patterns of ice-proximal lakes can therefore be used to constrain past ice-sheet histories (Austermann et al., 2020; Gowan et al., 2016; Lambeck et al., 2010, 2017). In turn, GIA may have influenced the depth and extent of proglacial lakes over the ice age through crustal deformation and gravitational perturbations.

Large proglacial lakes can affect summer air temperatures, delay summer ice ablation, moderate the timing and routing of ice melt, and potentially accelerate ice mass loss (Carrivick & Tweed, 2013). They can also impact regional to global climate—for example, abrupt drainage of proglacial lake Agassiz–Ojibway at 8.2 ka likely cooled the Northern Hemisphere by slowing Atlantic Ocean circulation (Barber et al., 1999; Wiersma &

Writing – review & editing: J. Austermann, A. D. Wickert, T. Pico, J. Kingslake, K. L. Callaghan, R. C. Creel

Renssen, 2006). Including proglacial lakes explicitly or as boundary conditions in ice-sheet models enhances ice loss through localized mechanical instabilities (Hinck et al., 2022; Quiquet et al., 2021; Sutherland et al., 2020), which Quiquet et al. (2021) termed "proglacial lake ice sheet instability" (PLISI). Modeling the Laurentide ice sheet, Quiquet et al. (2021) found that ice margins retreat faster when abutting proglacial lakes especially if the bedrock dips toward the ice interior (often due to ice loading). This finding suggests that proglacial lakes influence ice-sheet stability. Hinck et al. (2022) achieved similar results when implementing an adaptive proglacial lake boundary in the Parallel Ice Sheet Model. Since retreating ice sheets leave larger topographic depressions than advancing ones, it has been postulated that proglacial lakes form more frequently during deglaciations than glaciations, thereby contributing to the asymmetric shape—slow advances, rapid retreats—of Quaternary sea-level change (Fowler et al., 2013; Pollard, 1982).

Ice-sheet modeling studies that include proglacial lakes have provided critical insights into lake–ice-sheet interactions over the deglaciation, but don't include the full glacial cycle and are limited in a few substantial ways (Hinck et al., 2022; Quiquet et al., 2021; Sutherland et al., 2020). First, these models generally incorporate GIA through the ELRA (elastic lithosphere—relaxed asthenosphere) approximation, which doesn't capture gravitational effects and depth-varying mantle viscosity, and typically doesn't include ocean and lake loading. Second, numerical limitations often require coarse gridding, whereas drainage rerouting is controlled by fine topographic details (Wickert, 2016). Third, since observed ice-sheet margin locations are typically used to constrain but not produce physics-based ice-sheet models, the resulting ice-sheet model may not necessarily precisely match them. Lastly, lake-filling algorithms include some approximations—for example, requiring a certain fill rate to maintain numerical stability (Hinck et al., 2022) or filling lakes up to sea level rather than the spillway (Quiquet et al., 2021). In this study we address many of these limitations at the expense of not modeling ice-sheet physics. We focus on investigating how GIA has modulated lake geometry, depth, and volume around the Laurentide ice sheet over the last glacial cycle.

We extend the sea-level equation to include dynamically- and self-consistently-evolving proglacial lakes. Lakes form at the ice margin and drain from the lowest point in the topography; their water load deforms the solid Earth and alters its gravity field; and the overall ice-lake-ocean water budget is conserved over time. To model realistic lake locations and depths, we combine published ice-sheet reconstructions with higher resolution data on the margin of the Laurentide ice sheet. We compare predicted lake extents to paleolake shorelines to test the reconstruction's reliability. We then use the model to examine lake volumes, geometries, and depths over the glaciation versus the deglaciation in order to explore the role of GIA in shaping proglacial lakes and related implications for ice sheet stability.

2. Methods

To quantify how GIA shapes proglacial lakes, we extend the classical sea-level theory to self-consistently include proglacial lakes. We first describe the theory's extension to include lake water loads before detailing how proglacial lakes are calculated at each timestep. Lastly, we provide information on the inputs that this work uses.

2.1. Extension of the Sea Level Equation to Include Lake Loading

A generalized theory for calculating sea-level change due to ice-sheet change was first discussed by Farrell and Clark (1976) and later formulated by Mitrovica and Milne (2003). Kendall et al. (2005) developed an iterative algorithm to implement the sea-level equation through a gravitationally self-consistent formulation that accounts for migration of Earth's shorelines and rotation axis. We extend the formalism in two ways: (a) Proglacial lake changes are included in the load-change term, which affects Earth's gravity field, rotation axis, and regional deformation; (b) the global water budget between ice, oceans, and proglacial lakes is conserved by calculating ocean volume change as the difference between ice and proglacial-lake volume change. An overview of the algorithm focusing on our proglacial lake extension is provided in Text S1 in Supporting Information S1.

While this study focuses on proglacial lakes, we highlight that this algorithm and theory are extensible. First, it can be used to include any changes in terrestrial water storage (e.g., pluvial lakes or groundwater). Second, it can be combined with other sea-level equation extensions, including sediment redistribution (Dalca et al., 2013), sediment compaction (Ferrier et al., 2017; Pico et al., 2016), dynamic topography (Austermann & Mitrovica, 2015), or water flux across sills (Coulson et al., 2020).

2.2. Proglacial Lake Calculation

Within the algorithm, we calculate proglacial lake extent at each timestep for a given topography and ice margin. To do so, we first determine the current topography at 1 arcminute (approx. 1.8 km) resolution by deforming present-day topography (GEBCO Bathymetric Compilation Group, 2021) using calculated changes in global mean sea level (GMSL) and GIA. Such high resolution is necessary to adequately compute the shape and connectivity of depressions in the landscape. We sum this topography with ice-sheet thickness provided by the ice model in order to create a flow-routing surface (cf. Wickert, 2016). We then map landscape depressions (excluding ocean basins) using the Matlab function *imfill*. We next use the Matlab function *bwconncomp* to label and save only those depressions that intersect the ice sheet margin, removing depressions away from or on top of the ice sheet. The remaining depressions are filled up to their lowest spill points. This calculation, performed at each timestep, allows computing the change in lake load. We then downsample the load change to the resolution of the GIA calculation and feed it back into the sea-level algorithm. Similar proglacial lake-filling schemes have been developed and explored in the past (Berends & van de Wal, 2016; Hinck et al., 2020; Lambeck et al., 2017).

Our approach assumes three premises. First, ice melt or precipitation fills every ice-marginal depression with water; this accords with observations of North America's proglacial lakes (e.g., Breckenridge, 2015; C. F. M. Lewis et al., 2008). Second, we neglect geomorphological processes (i.e., erosion and deposition) that may affect lake drainage over the glacial cycle. This is justified since, unlike in pluvial settings (Shroder et al., 2016), geomorphic evolution is generally thought to be caused by spillway development rather than driving it (e.g., Curry et al., 2021; Fisher, 2020; Pico et al., 2022). Third, we neglect groundwater changes and its respective load, which we expect to accompany both general climatic change and surface-water changes related to proglacial lake evolution.

2.3. Input Ice Sheet Model and Viscosity Structure

Our calculations require as input (a) present-day topography (Amante, 2009), (b) an ice-sheet reconstruction, and (c) elastic and viscous properties of the Earth's interior. For the deglaciation we combine an ice-sheet reconstruction of the Laurentide by Lambeck et al. (2017) with a reconstruction of the Fennoscandian ice sheet by Lambeck et al. (2006); Lambeck et al. (2010), the British–Irish ice sheet by Lambeck (1995); Lambeck (1996); Lambeck et al. (1996), and the remaining ice sheets by Peltier et al. (2015). This results in the most up-to-date combined ice history by K. Lambeck and his colleagues, which we choose because they used proglacial lake shorelines to constrain their Laurentide reconstruction. From MIS 5e to the Last Glacial Maximum (LGM)–henceforth referred to as the glaciation unless noted otherwise–we adopt the ICE-PC GMSL history (Pico et al., 2016), which has relatively low ice volume during MIS 3 and incorporates ice-volume constraints during MIS 5a–5d from Creveling et al. (2017, Figure 1a). For each timestep of the glaciation, we then use the ice geometry from the deglaciation that matches the glacial ice volume. We note that this is a simplification, given that ice growth likely led to ice sheets that differed in shape from those developed during ice collapse (e.g., Kleman et al., 2002).

To accurately model proglacial lakes, we adjust the modeled margin of the Laurentide ice sheet to follow the detailed (0.5–6.5 km resolution) reconstruction by Dalton et al. (2020) and note that the exact location of their ice margin is resolved to varying degree. We first linearly interpolate the original ice reconstructions onto the timescale of Dalton et al. (2020), who recalibrated radiocarbon ages using IntCal13 (Reimer et al., 2013) and assumed an error of approx. 10%. We then extend the ice sheet with a thickness of 500 m where the Dalton et al. (2020) ice-sheet margin lies outside the margin of the original ice sheet model. This thickness is chosen to not allow water ponding on the ice sheet (lakes are generally less than 500 m deep at the ice margin) while simultaneously keeping mass changes to the ice reconstruction minimal given that these are constructed to fit GIA-related observations. If the ice margin by Dalton et al. (2020) shows that the ice sheet had a smaller extent, we remove ice lying beyond their margin. This is done at 1-arcminute resolution to produce a high-resolution ice-sheet reconstruction for the proglacial-lakes calculation, and alters total ice volume by less than 2%. During the glaciation, we use the ice margin from the deglaciation time step that is closest to the ice volume during the glaciation.

Finally, the ice-sheet model is downsampled to a Gauss Legendre grid with maximum degree 256 for the GIA calculation, which corresponds to a spatial resolution of approx. 78 km (half wavelength). This forms our default ice history, which we call LAM-PC when referring to the whole glacial cycle and LAM when referring to the deglaciation.

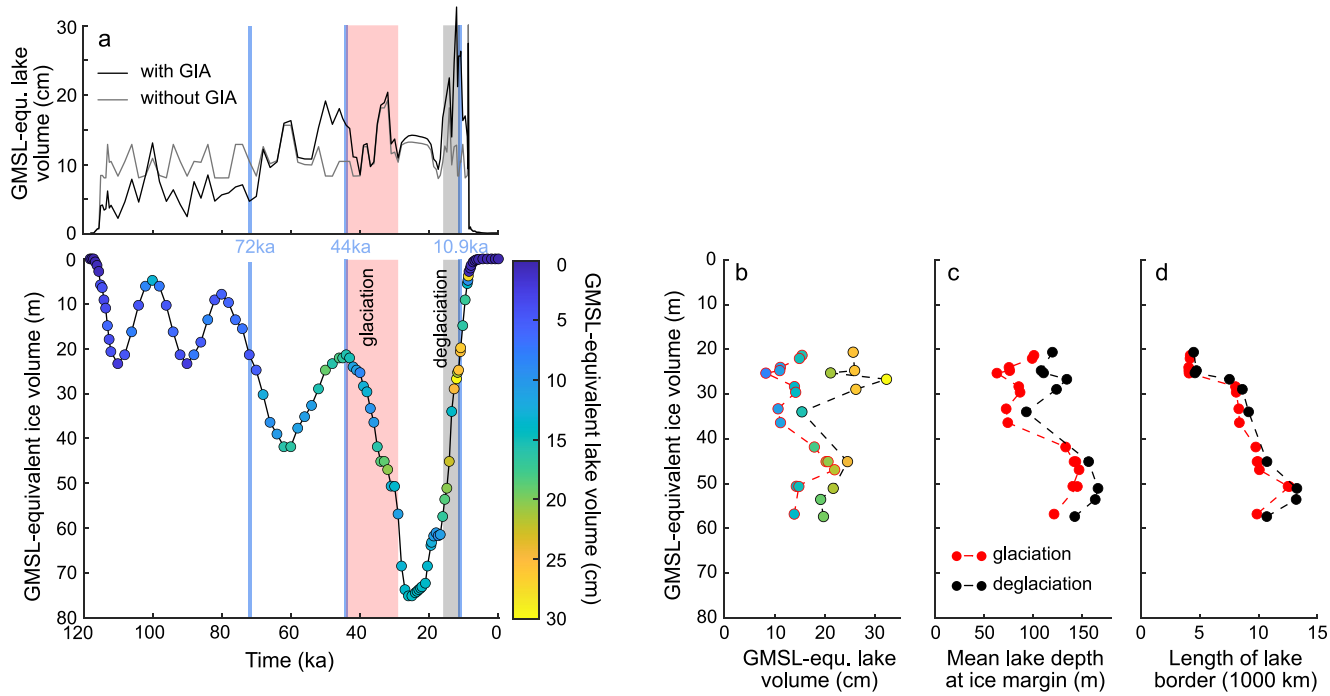

Figure 1. *Volume of Laurentide ice sheet and characteristics of its proglacial lakes*. (a) Global mean sea level (GMSL)-equivalent lake volume changes in the LAM-PC simulation. Top shows results comparing a simulation with (black) and without (gray) glacial isostatic adjustment. Bottom shows the GMSL-equivalent ice-volume change of the Laurentide ice sheet with lake volume changes shown as colored markers. One meter of GMSL equals ~3.6×10^5 km^3 of meltwater. Vertical bands denote periods of the glaciation (red) and deglaciation (gray) used in panels (b–d). Blue vertical lines show time slices used in Figure 2. (b) GMSL-equivalent lake volume as a function of ice volume for the glaciation (red dashed line) and deglaciation (black dashed line). Colored markers denote the GMSL-equivalent lake volume (same as *x*-axis). (c) Mean proglacial lake depth at the ice margin for the glaciation (red) and deglaciation (black). (d) Length of ice margin that borders proglacial lakes for the glaciation (red) and deglaciation (black).

We perform several sensitivity tests. First, we explore how GIA affects the lakes by running a simulation without GIA, which means the topography does not deform over time. Second, we run a simulation without lake-loading to isolate its effect. Third, we explore how our results change if we assume a different ice geometry. To do so we use the ice model ICE-7G (Roy & Peltier, 2018) for the deglaciation and then proceed as described for our LAM-PC run (i.e., we adjust the ice margin following Dalton et al. (2020) and construct a glaciation phase following ICE-PC Pico et al. (2016)). Lastly, four additional sensitivity tests that explore variations in viscosity, resolution, and the glacial GMSL history are described in Text S2 in Supporting Information S1.

For the viscosity we use a radially symmetric structure with a lithospheric thickness of 96 km, an upper mantle viscosity of 5×10^{20} Pa s and a lower mantle viscosity of 15×10^{21} Pa s. This is close to the best-fitting parameters from Lambeck et al. (2017). When calculating relative sea level with ICE-7G, we use the VM5a viscosity structure (Peltier et al., 2015). For the elastic structure we assume PREM (Dziewonski & Anderson, 1981).

3. Results and Discussion

Our simulations produce proglacial lakes around the Laurentide ice sheet with a GMSL-equivalent volume of up to 30 cm when applying the LAM ice model (Figure 1a, Movie S1) and up to 45 cm when applying ICE-7G (Figure S1a in Supporting Information S1). Lake volumes are generally highest during the rapid deglaciation (ca. 14–11 ka), corresponding to times when major proglacial lakes extended along the northern (Lake McConnell: Smith, 1994), mid-latitude (Lake Agassiz: e.g., Breckenridge, 2015; Lepper et al., 2013; Teller & Leverington, 2004), and southern Laurentide ice sheet borders (Lakes Duluth/Superior: Breckenridge, 2013; Algonquin: Larsen, 1987; Iroquois–Ontario and Ojibway: Breckenridge et al., 2012; Muller & Calkin, 1993; Muller & Prest, 1985) (see Figure 2c for the location of some of these lakes). Our simulation produces proglacial lakes that generally fit observations of past lake extent (Figure S2 in Supporting Information S1). Lake volumes vary less and peak at lower values when GIA is not accounted for (gray curve in Figure 1a).

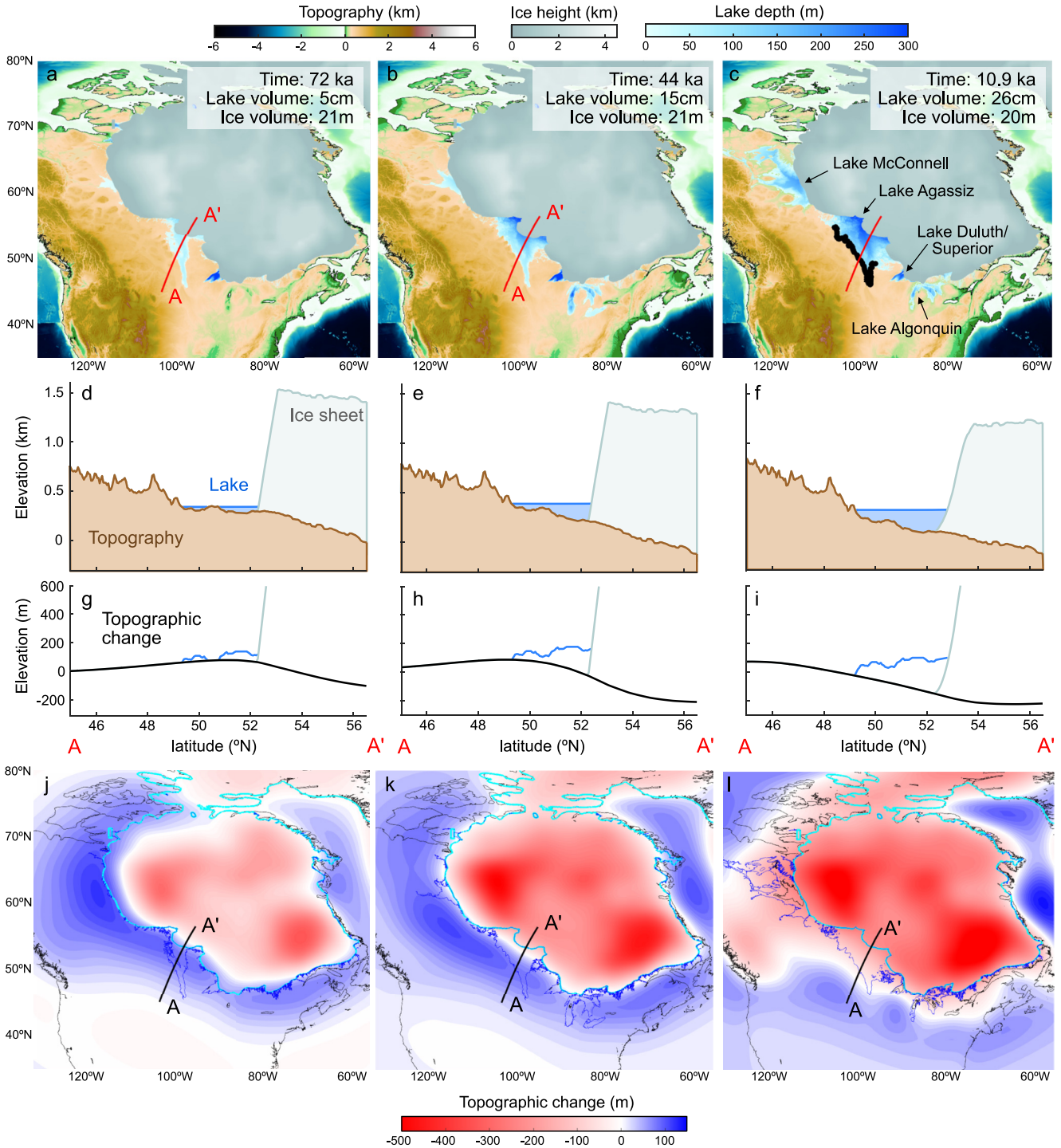

Figure 2. *Lake reconstruction at three different stages of glacial isostatic deformation*. (a–c) Map of topography, ice sheet, and proglacial lakes for the LAM-PC simulation at 72, 44, and 10.9 ka, respectively. Upper Campbell shorelines are marked in black from Gowan et al. (2016) in panel (c). Red lines mark cross sections for panels (d–i). The global mean sea level-equivalent lake-volume and ice-volume change is stated in each panel. (d–f) Cross section through the topography (brown), ice sheet (gray), and proglacial lake surface (blue) at 72, 44, and 10.9 ka, respectively. (g–i) Topographic change (relative to today) driven by glacial isostatic adjustment at 72, 44, and 10.9 ka, respectively (black line). The ice sheet (gray) and lake thickness (blue) is shown on top of the relative topography. (j–l) Topographic change (relative to today) at 72, 44, and 10.9 ka, respectively (contours denote 10 m, note the non-linear colorscale). Ice margins (cyan), lake margins (blue), and coastlines (black) are shown at the respective times.

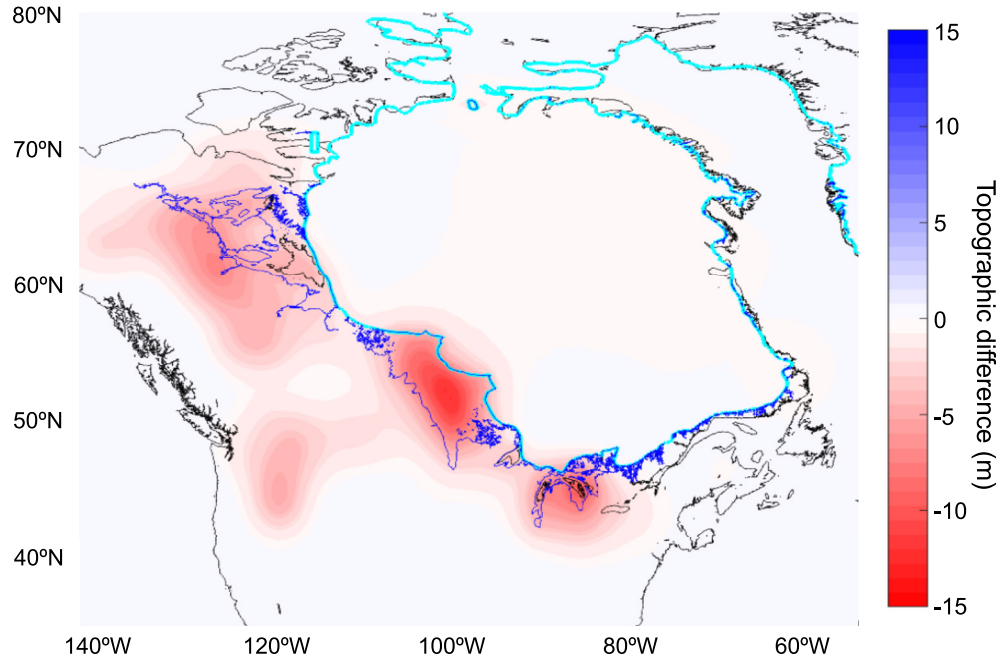

Figure 3. *Deformation due to lake loading at 10.9 ka*. Difference in topography at 10.9 ka between a simulation that includes lake loading and one that does not. Ice margins (cyan), lake margins (blue), and coastlines (black) at 10.9 ka are shown.

The best-documented Laurentide proglacial lake shoreline is the Upper Campbell shoreline of Lake Agassiz (Figure 2c), which dates to 10.5 ± 0.3 ka (see Breckenridge, 2015, and references therein). Ice-sheet margins are constrained at 10.9 and 10.3 ka (Dalton et al., 2020). Our LAM simulation only produces a lake matching the shoreline geometry at 10.9 ka, which indicates at least one of three things: (a) the lake ages are on the older end of the range constrained by the optically stimulated luminescence chronology (Lepper et al., 2013), (b) the age of the ice margin is actually younger (note that the age of the 10.9 ka ice margin has an uncertainty of approx. 0.5 kyr, Dalton et al., 2020), and/or (c) retreat occurred nearer to 10.3 than to 10.9 ka. Using ICE-7G produces a lake that is too small during either time, perhaps due to a steeper peripheral bulge or a lower spill point. GIA has deformed the shorelines of Lake Agassiz, and our predictions of the tilt at 10.9 ka resemble the observed ones when using the LAM ice model (Figure S3 in Supporting Information S1).

Another time of large lake volume in both the LAM and the ICE-7G ice model is 8.7 ka, after which lake volume drops to near zero. This is a result of ice retreat into Hudson Bay, which creates space for a sizable proglacial lake before the ice bridge collapses (see Movie S1). This behavior aligns with the abrupt drainage of proglacial Lake Agassiz-Ojibway at 8.2 ka, which slowed Atlantic circulation (Barber et al., 1999; Wiersma & Renssen, 2006). The modeled lake drains at 8.5 ka (instead of 8.2 ka) due to the prescribed ice bridge collapse at this time (Dalton et al., 2020).

The water load of proglacial lakes not only contributes to the ice–ocean–terrestrial-water budget, but also deforms the solid Earth and gravity field. Deformation caused by lake loading (e.g., at 10.9 ka, as shown in Figure 2c) deflects topography by up to 15 m in the center of the former lake and 2–8 m at its periphery (Figure 3, Figure S3 in Supporting Information S1). Due to viscoelastic delay in the GIA response, deformation due to lake loading is not confined to locations of contemporaneous lakes, but also reflects former lakes that have since drained (Figure 3).

3.1. Comparing Lakes Between the Glaciation and Deglaciation

The volume and shape of proglacial lakes is affected by broad-scale ice load-driven topographic deformation and by shorter wavelength local topography, which together determine the extent of basins and height of sills along with their evolution through time. To assess the role of GIA on proglacial lake volume and shape, we compare times when the Laurentide ice sheet size and margins are similar but glacial history varies. Since the

GIA signal depends on the history of loading, differences in prior loading will produce differences in topography (and proglacial lakes) during ice growth versus ice retreat.

Figure 2 shows the deformation caused by GIA and the resulting lake distribution and depth at three times with almost identical ice sheets in our LAM-PC simulation: 72, 44, and 10.9 ka. At the earliest time (72 ka), the ice sheet was growing, which means that the peripheral bulge was migrating outwards as the ice margin expanded. As a result, the peripheral bulge remained close to the Laurentide ice sheet; little GIA-driven depression existed around the ice margin; and only small proglacial lakes formed (Figures 2a, 2d, 2g, and 2j). In fact, the position of the peripheral bulge even hindered the formation of proglacial lakes in the early part of the glacial cycle (Figure 1a). Lakes at 72 ka held a total GMSL-equivalent volume of 5 cm. The ice sheet continued to grow through MIS 4 (~60 ka) before retreating to an MIS 3 minimum extent (~44 ka). This retreat caused the peripheral bulge to be further outward of the ice sheet, leaving a modest depression, which produced proglacial lakes with a GMSL-equivalent volume of 15 cm (Figures 2b, 2e, 2h, and 2k). After MIS 3, the Laurentide ice sheet grew to its MIS 2 maximum extent (achieved 26–19.5 ka, Clark et al., 2009) before it retreated during the deglaciation. This rapid retreat separated the ice margin and peripheral bulge (Figures 2c, 2f, 2i, and 2l), thereby accommodating a larger GMSL-equivalent lake volume of 26 cm.

The lagged peripheral-bulge response to ice-margin change causes proglacial lake depths and volumes to be consistently higher during rapid ice-sheet retreat (16–11 ka) than during ice advance (44–29 ka, Figure 1b). Ice volumes and margins at 28 and 12.1 ka were nearly identical, but the proglacial lakes during ice retreat held over twice as much water: 32 cm GMSL-equivalent at 12.1 ka versus 14 cm at 28 ka. This excess volume is caused by GIA (Figure 1a). The mean depth of proglacial lakes at the ice margin is consistently larger during the deglaciation (Figure 1c, black markers) than during the glaciation (Figure 1c, red markers). The same, but to a lesser degree, holds for the length of ice margin that borders proglacial lakes (Figure 1d). The difference in lake depth is largest for smaller ice volumes (20–30 m of GMSL-equivalent ice volume), where the average lake depth along the ice margin increases by 50 m (at a GMSL-equivalent ice volume of 28 m). Differences are smaller but still notable at higher ice volumes.

The ICE-7G ice history produces even more pronounced lake volume differences between the glaciation and deglaciation (Figure S1 in Supporting Information S1). This difference might be caused by a generally larger Laurentide ice sheet compared to LAM. At a GMSL-equivalent ice volume of 35 m, the lake volume is three times larger during the deglaciation than the glaciation and proglacial lakes are on average twice as deep along the ice margin. The difference in average lake depth along the margin for the same GMSL-equivalent ice volume is consistently on the order of 50 m when comparing the glaciation and deglaciation phases (Figure S1c in Supporting Information S1). Varying the glaciation phase indicates that a history of (intermittent) ice retreat during the glaciation, rather than the pacing of ice advance, most impacts the lake volume by creating an expansive topographic depression around the ice sheet (Figure S4 and Text S2 in Supporting Information S1).

Deeper water during the deglaciation may produce a positive feedback that further speeds ice retreat and deepens proglacial lakes. However, this feedback can break down quickly if the ice sheet opens up a lower spill point for the lake. For marine-based ice sheets, the ice flux at the grounding line is nonlinearly proportional to water depth (Schoof, 2007). If lakes drive ice loss through similar processes, the 50 m depth difference between proglacial lakes during the deglaciation (~135 m) versus the glaciation (~85 m), at a GMSL-equivalent ice volume of 28 m, would drive a significantly increased ice flux. For example, if the Schoof (2007) grounding-line parameterization is assumed, which predicts that ice flux is proportional to water depth to the power of 4.75 (Robel et al., 2018), the outflux across the ice margin during the deglaciation would increase by a factor of 9. When the bedrock slopes toward the ice-sheet interior (Figures 2d–2f), as is exacerbated by GIA during the deglaciation, the ice margin may be even more susceptible to retreat, especially when lakes have already reached a significant depth (Quiquet et al., 2021).

Numerical ice sheet models that don't fill proglacial lakes up to the respective sill or don't account for lake loading will predict shallower lake depths at the ice margin and hence underestimate the influence of proglacial lakes on Laurentide ice mass change. Future ice sheet modeling efforts should therefore include self-consistent proglacial lakes and the algorithm derived here provides a means to do so, especially if the ice sheet model is already coupled to GIA (e.g., Gomez et al., 2013).

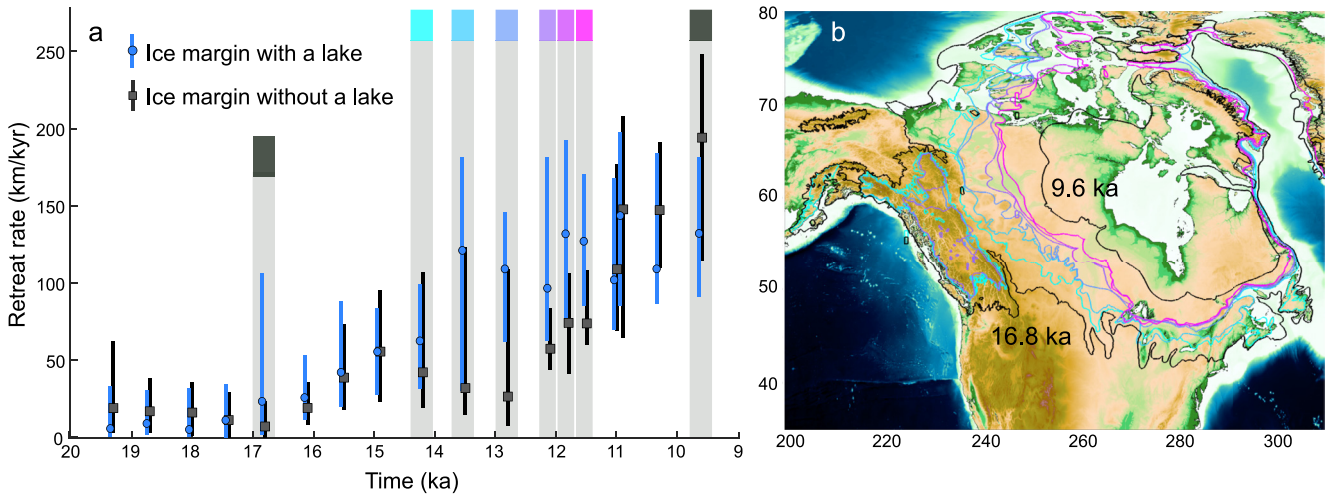

Figure 4. *Ice retreat at margins with and without proglacial lakes*. (a) Retreat rate of the ice margin as a function of time. Black markers and lines show the retreat rate for ice margins that do not have bordering proglacial lakes, the marker shows the 50th percentile and the line shows the range from the 25th to the 75th percentile. Blue markers show the same for ice margins that have bordering proglacial lakes. Blue markers are slightly offset for visual purposes. (b) Location of the ice margin at different times during the deglaciation, colors correspond to the time slices highlighted in panel (a). Present-day topography is shown for reference. See Figure S6 in Supporting Information S1 for a version that includes retreat rates in marine-based sectors.

3.2. Proglacial Lakes and Ice-Sheet Retreat

We explore whether ice-margin segments that border proglacial lakes retreat faster than those that do not. In this analysis we only consider lakes that are at least 20 m deep at the ice margin. We calculate each ice-margin segment's retreat rate as the average between the retreat prior to and following the current timestep (note that we do not propagate uncertainties in the ice margin age). We group ice margins with and without proglacial lakes, then extract the 25th, 50th, and 75th percentile of each timestep's retreat rate (Figure 4). Retreat rates, slow at the deglaciation's onset, accelerate starting ∼16.5 ka. No significant difference occurs between ice margins with and without proglacial lakes prior to 16.5 ka (blue vs. black markers in Figure 4a). From 14.2 until ∼11.5 ka, however, ice-margin retreat is significantly faster at margins that border proglacial lakes. During this time, the ice margin retreats across the flat interior of northern North America, which allows large proglacial lakes to form (Figures 2c and 4b). During the Holocene, the ice margin continues to retreat rapidly regardless of the presence of proglacial lakes. The percentage of continent interior-facing ice margin that is bordered by a proglacial lake increases from 18 to around 16 ka, then remains high (around 60%). The lakes' average depth at the ice margin decreases in the early Holocene (from around 150 to 90 m between 11 and 10.3 ka). Our results are qualitatively unchanged when the ICE-7G ice model is considered (Figure S5 in Supporting Information S1).

This analysis demonstrates that there are periods when proglacial lake existence correlates with faster ice margin retreat, which aligns with results from ice sheet modeling (Quiquet et al., 2021). This finding suggests a positive ice-retreat feedback where lakes drive faster retreat, which in turn produces more accommodation space for larger lakes to form. However, this mechanism is geographically limited to relatively flat regions with overall reverse bed slopes where GIA-associated deformation is comparable to the topographic relief.

4. Conclusion

The conceptual role of GIA in proglacial lake formation has long been recognized. Here we quantify how GIA modulates Laurentide ice sheet-proximal lake geometry, depth, and volume over the last glacial cycle. We adapt higher resolution ice-margin data (Dalton et al., 2020) and a GIA model to capture proglacial-lake evolution between MIS5e and today. We find that Laurentide-proximal lakes have volumes up to 45 cm GMSL-equivalent sea level and deform topography by up to tens of meters. These estimates might further increase if the model included proglacial lake-driven groundwater changes.

We find that the location of the Laurentide's peripheral bulge strongly influences the geometry of North American proglacial lakes during the onset of glaciation and the deglaciation. Proglacial lake volumes during the

deglaciation can be 5 times larger than corresponding glacial volumes with equivalent ice sheet size because the deglaciation is associated with a more-extensive peripheral bulge with a larger depression around the ice sheet. Average ice-marginal lake depths during deglacial phases are typically 20–50 m deeper, and up to 90 m deeper, than those from ice-advance phases with similar ice margins and volumes. GIA most strongly influences proglacial lake geometry in low-relief landscapes with reverse bed slopes, and the presence of these GIA-enlarged lakes at 14.2–11.5 ka correlates with faster ice-margin retreat. Our results support the idea that coupled lake growth and ice-margin retreat through PLISI likely contributed to rapid collapse of the Laurentide ice sheet (Hinck et al., 2022; Quiquet et al., 2021) and the asymmetric shape of ice age sea level variability (Fowler et al., 2013; Pollard, 1982).

Data Availability Statement

The code used to produce the modeling is available on github (jaustermann/SLcode/tree/master/GRL_2022_proglacial_lakes). The data used to constrain the ice margin is from Dalton et al. (2020). Input ice reconstructions and topography as well as output sea level and lake geometries can be found on Zenodo (https://doi.org/10.5281/zenodo.7378941).

Acknowledgments
This material is based upon work supported by NSF Grant EAR-1903518 and EAR-1903606 (JA, ADW, and KLC). ADW received further support through a research fellowship from the Alexander von Humboldt Foundation. TP received support from NSF EAR-2120574. JA acknowledges support from the Vetlesen Foundation. We acknowledge computing resources from Columbia University's Shared Research Computing Facility project, which is supported by NIH Research Facility Improvement Grant 1G20RR030893-01, and associated funds from the New York State Empire State Development, Division of Science Technology and Innovation (NYSTAR) Contract C090171, both awarded 15 April 2010. We thank Jerry X. Mitrovica for initial discussions and Joshua Cuzzone, Lambert Caron, and an anoymous reviewer for their useful feedback.

References

Amante, C. (2009). *ETOPO1 arc-minute global relief model: Procedures, data sources and analysis*. National Geophysical Data Center, NOAA. https://doi.org/10.7289/V5C8276M. Retrieved from https://data.nodc.noaa.gov/cgi-bin/iso?id=gov.noaa.ngdc.mgg.dem:316

Austermann, J., Chen, C., Lau, H., Maloof, A., & Latychev, K. (2020). Constraints on mantle viscosity and Laurentide ice sheet evolution from pluvial paleolake shorelines in the western United States. *Earth and Planetary Science Letters*, *532*, 116006. https://doi.org/10.1016/j.epsl.2019.116006

Austermann, J., & Mitrovica, J. X. (2015). Calculating gravitationally self-consistent sea level changes driven by dynamic topography. *Geophysical Journal International*, *203*(3), 1909–1922. https://doi.org/10.1093/gji/ggv371

Barber, D. C., Dyke, A., Hillaire-Marcel, C., Jennings, A. E., Andrews, J. T., Kerwin, M. W., et al. (1999). Forcing of the cold event of 8,200 years ago by catastrophic drainage of Laurentide lakes. *Nature*, *400*(6742), 344–348. https://doi.org/10.1038/22504

Berends, C. J., & van de Wal, R. S. W. (2016). A computationally efficient depression-filling algorithm for digital elevation models, applied to proglacial lake drainage. *Geoscientific Model Development*, *9*(12), 4451–4460. https://doi.org/10.5194/gmd-9-4451-2016

Breckenridge, A. (2013). An analysis of the late glacial lake levels within the western Lake Superior basin based on digital elevation models. *Quaternary Research*, *80*(3), 383–395. https://doi.org/10.1016/j.yqres.2013.09.001

Breckenridge, A. (2015). The Tintah-Campbell gap and implications for glacial Lake Agassiz drainage during the Younger Dryas cold interval. *Quaternary Science Reviews*, *117*, 124–134. https://doi.org/10.1016/j.quascirev.2015.04.009

Breckenridge, A., Lowell, T. V., Stroup, J. S., & Evans, G. (2012). A review and analysis of varve thickness records from glacial Lake Ojibway (Ontario and Quebec, Canada). *Quaternary International*, *260*, 43–54. https://doi.org/10.1016/j.quaint.2011.09.031. Retrieved from https://www.sciencedirect.com/science/article/pii/S1040618211005581

Carrivick, J. L., & Tweed, F. S. (2013). Proglacial lakes: Character, behaviour and geological importance. *Quaternary Science Reviews*, *78*, 34–52. https://doi.org/10.1016/j.quascirev.2013.07.028

Clark, P. U., Dyke, A. S., Shakun, J. D., Carlson, A. E., Clark, J., Wohlfarth, B., et al. (2009). The last glacial maximum. *Science*, *325*(5941), 710–714. https://doi.org/10.1126/science.1172873

Coulson, S., Al-Attar, D., & Mitrovica, J. (2020). An extended ice-age sea-level equation: Incorporating water flux across sills. *Geophysical Journal International*, *225*(1), 236–252. https://doi.org/10.1093/gji/ggaa596

Creveling, J. R., Mitrovica, J. X., Clark, P. U., Waelbroeck, C., & Pico, T. (2017). Predicted bounds on peak global mean sea level during marine isotope stages 5a and 5c. *Quaternary Science Reviews*, *163*, 193–208. https://doi.org/10.1016/j.quascirev.2017.03.003

Curry, B. B., Kehew, A. E., Antinao, J. L., Esch, J., Huot, S., Caron, O. J., & Thomason, J. F. (2021). Deglacial Kankakee Torrent, source to sink. In *Untangling the Quaternary Period—A Legacy of Stephen C. Porter*. Geological Society of America. https://doi.org/10.1130/2020.2548(16)

Dalca, A. V., Ferrier, K. L., Mitrovica, J. X., Perron, J. T., Milne, G. A., & Creveling, J. R. (2013). On postglacial sea level—III. Incorporating sediment redistribution. *Geophysical Journal International*, *194*(1), 45–60. https://doi.org/10.1093/gji/ggt089

Dalton, A. S., Margold, M., Stokes, C. R., Tarasov, L., Dyke, A. S., Adams, R. S., et al. (2020). An updated radiocarbon-based ice margin chronology for the last deglaciation of the North American Ice Sheet Complex. *Quaternary Science Reviews*, *234*, 106223. https://doi.org/10.1016/j.quascirev.2020.106223

Dziewonski, A. M., & Anderson, D. L. (1981). Preliminary reference Earth model. *Physics of the Earth and Planetary Interiors*, *25*(4), 297–356. https://doi.org/10.1016/0031-9201(81)90046-7

Farrell, W. E., & Clark, J. A. (1976). On postglacial sea level. *Geophysical Journal International*, *46*(3), 647–667. https://doi.org/10.1111/j.1365-246x.1976.tb01252.x

Ferrier, K. L., Austermann, J., Mitrovica, J. X., & Pico, T. (2017). Incorporating sediment compaction into a gravitationally self-consistent model for ice age sea-level change. *Geophysical Journal International*, *211*(1), 663–672. https://doi.org/10.1093/gji/ggx293

Fisher, T. G. (2020). Megaflooding associated with glacial Lake Agassiz. *Earth-Science Reviews*, *201*, 102974. https://doi.org/10.1016/j.earscirev.2019.102974

Fowler, A. C., Rickaby, R. E. M., & Wolff, E. W. (2013). Exploration of a simple model for ice ages. *GEM-International Journal on Geomathematics*, *4*(2), 227–297. https://doi.org/10.1007/s13137-012-0040-7

GEBCO Bathymetric Compilation Group. (2021). *The GEBCO_2021 Grid - a continuous terrain model of the global oceans and land*. NERC EDS British Oceanographic Data Centre NOC. https://doi.org/10.5285/C6612CBE-50B3-0CFF-E053-6C86ABC09F8F. Retrieved from https://www.bodc.ac.uk/data/published_data_library/catalogue/10.5285/c6612cbe-50b3-0cff-e053-6c86abc09f8f/

Gomez, N., Pollard, D., & Mitrovica, J. X. (2013). A 3-D coupled ice sheet—Sea level model applied to Antarctica through the last 40 ky. *Earth and Planetary Science Letters*, *384*, 88–99. https://doi.org/10.1016/j.epsl.2013.09.042
Gorlach, A., Hang, T., & Kalm, V. (2017). GIS-based reconstruction of Late Weichselian proglacial lakes in northwestern Russia and Belarus. *Boreas*, *46*(3), 486–502. https://doi.org/10.1111/bor.12223
Gowan, E. J., Tregoning, P., Purcell, A., Montillet, J.-P., & McClusky, S. (2016). A model of the western Laurentide Ice Sheet, using observations of glacial isostatic adjustment. *Quaternary Science Reviews*, *139*, 1–16. https://doi.org/10.1016/j.quascirev.2016.03.003
Hinck, S., Gowan, E. J., & Lohmann, G. (2020). LakeCC: A tool for efficiently identifying lake basins with application to palaeogeographic reconstructions of North America. *Journal of Quaternary Science*, *35*(3), 422–432. https://doi.org/10.1002/jqs.3182
Hinck, S., Gowan, E. J., Zhang, X., & Lohmann, G. (2022). PISM-LakeCC: Implementing an adaptive proglacial lake boundary in an ice sheet model. *The Cryosphere*, *16*(3), 941–965. https://doi.org/10.5194/tc-16-941-2022
Kendall, R. A., Mitrovica, J. X., & Milne, G. A. (2005). On post-glacial sea level–II. Numerical formulation and comparative results on spherically symmetric models. *Geophysical Journal International*, *161*(3), 679–706. https://doi.org/10.1111/j.1365-246x.2005.02553.x
Kleman, J., Fastook, J., & Stroeven, A. P. (2002). Geologically and geomorphologically constrained numerical model of Laurentide Ice Sheet inception and build-up. *Quaternary International*, *95–96*, 87–98. https://doi.org/10.1016/s1040-6182(02)00030-7
Lambeck, K. (1995). Late Devensian and Holocene shorelines of the British Isles and North Sea from models of glacio-hydro-isostatic rebound. *Journal of the Geological Society*, *152*(3), 437–448. https://doi.org/10.1144/gsjgs.152.3.0437
Lambeck, K. (1996). Glaciation and sea-level change for Ireland and the Irish Sea since Late Devensian/Midlandian time. *Journal of the Geological Society*, *153*(6), 853–872. https://doi.org/10.1144/gsjgs.153.6.0853
Lambeck, K., Johnston, P., Smither, C., & Nakada, M. (1996). Glacial rebound of the British Isles-III. Constraints on mantle viscosity. *Geophysical Journal International*, *125*(2), 340–354. https://doi.org/10.1111/j.1365-246x.1996.tb00003.x
Lambeck, K., Purcell, A., Funder, S., Kjær, K., Larsen, E., & Möller, P. (2006). Constraints on the Late Saalian to early Middle Weichselian ice sheet of Eurasia from field data and rebound modelling. *Boreas*, *35*(3), 539–575. https://doi.org/10.1080/03009480600781875
Lambeck, K., Purcell, A., Zhao, J., & Svensson, N.-O. (2010). The Scandinavian ice sheet: From MIS 4 to the end of the last glacial maximum. *Boreas*, *39*(2), 410–435. https://doi.org/10.1111/j.1502-3885.2010.00140.x
Lambeck, K., Purcell, A., & Zhao, S. (2017). The North American Late Wisconsin ice sheet and mantle viscosity from glacial rebound analyses. *Quaternary Science Reviews*, *158*, 172–210. https://doi.org/10.1016/j.quascirev.2016.11.033
Larsen, C. E. (1987). *Geological history of glacial lake Algonquin and the upper Great Lakes* (USGS Numbered Series). U.S. Geological Survey, Federal Center, USGS. Box 25425.
Lepper, K., Buell, A. W., Fisher, T. G., & Lowell, T. V. (2013). A chronology for glacial Lake Agassiz shorelines along Upham's namesake transect. *Quaternary Research*, *80*(1), 88–98. https://doi.org/10.1016/j.yqres.2013.02.002
Lewis, C. F. M., Karrow, P. F., Blasco, S. M., McCarthy, F. M. G., King, J. W., Moore, T. C., & Rea, D. K. (2008). Evolution of lakes in the Huron basin: Deglaciation to present. *Aquatic Ecosystem Health and Management*, *11*(2), 127–136. https://doi.org/10.1080/14634980802095263
Lewis, M., Breckenridge, A., & Teller, J. (2021). Reconstruction of isostatically-adjusted paleo-strandlines along the southern margin of the Laurentide Ice Sheet in the Great Lakes, Lake Agassiz and Champlain Sea basins. *Canadian Journal of Earth Sciences*, *59*(11), 826–846. https://doi.org/10.1139/cjes-2021-0005
Mangerud, J., Jakobsson, M., Alexanderson, H., Astakhov, V., Clarke, G. K., Henriksen, M., & Svendsen, J. I. (2004). Ice-dammed lakes and rerouting of the drainage of northern Eurasia during the Last Glaciation. *Quaternary Science Reviews*, *23*(11–13), 1313–1332. https://doi.org/10.1016/j.quascirev.2003.12.009
Mitrovica, J. X., & Milne, G. A. (2003). On post-glacial sea level: I. General theory. *Geophysical Journal International*, *154*(2), 253–267. https://doi.org/10.1046/j.1365-246x.2003.01942.x
Muller, E., & Calkin, P. (1993). Timing of Pleistocene events in New York state. *Canadian Journal of Earth Sciences*, *30*(9), 1829–1845. https://doi.org/10.1139/e93-161
Muller, E. H., & Prest, V. K. (1985). Quaternary evolution of the great lakes. In P. F. Karrow & P. E. Calkin (Eds.), *Quaternary evolution of the great lakes* (pp. 213–229). Geological Association of Canada.
Murton, D. K., & Murton, J. B. (2012). Middle and Late Pleistocene glacial lakes of lowland Britain and the southern North Sea basin. *Quaternary International*, *260*, 115–142. https://doi.org/10.1016/j.quaint.2011.07.034
Peltier, W. R., Argus, D. F., & Drummond, R. (2015). Space geodesy constrains ice age terminal deglaciation: The global ICE-6G_C (VM5a) model. *Journal of Geophysical Research: Solid Earth*, *120*(1), 450–487. https://doi.org/10.1002/2014jb011176
Pico, T., David, S. R., Larsen, I. J., Mix, A. C., Lehnigk, K., & Lamb, M. P. (2022). Glacial isostatic adjustment directed incision of the Channeled Scabland by Ice Age megafloods. *Proceedings of the National Academy of Sciences of the United States of America*, *119*(8), e2109502119. https://doi.org/10.1073/pnas.2109502119
Pico, T., Mitrovica, J., Ferrier, K., & Braun, J. (2016). Global ice volume during MIS 3 inferred from a sea-level analysis of sedimentary core records in the Yellow River Delta. *Quaternary Science Reviews*, *152*, 72–79. https://doi.org/10.1016/j.quascirev.2016.09.012
Pollard, D. (1982). A simple ice sheet model yields realistic 100 kyr glacial cycles. *Nature*, *296*(5855), 334–338. https://doi.org/10.1038/296334a0
Quiquet, A., Dumas, C., Paillard, D., Ramstein, G., Ritz, C., & Roche, D. M. (2021). Deglacial ice sheet instabilities induced by proglacial lakes. *Geophysical Research Letters*, *48*(9), e2020GL092141. https://doi.org/10.1029/2020gl092141
Reimer, P. J., Bard, E., Bayliss, A., Beck, J. W., Blackwell, P. G., Ramsey, C. B., et al. (2013). IntCal13 and Marine13 radiocarbon age calibration curves 0–50,000 years cal BP. *Radiocarbon*, *55*(4), 1869–1887. https://doi.org/10.2458/azu_js_rc.55.16947
Robel, A. A., Roe, G. H., & Haseloff, M. (2018). Response of marine-terminating glaciers to forcing: Time scales, sensitivities, instabilities, and stochastic dynamics. *Journal of Geophysical Research: Earth Surface*, *123*(9), 2205–2227. https://doi.org/10.1029/2018jf004709
Roy, K., & Peltier, W. (2018). Relative sea level in the Western Mediterranean basin: A regional test of the ICE-7G_NA (VM7) model and a constraint on late Holocene Antarctic deglaciation. *Quaternary Science Reviews*, *183*, 76–87. https://doi.org/10.1016/j.quascirev.2017.12.021
Schoof, C. (2007). Ice sheet grounding line dynamics: Steady states, stability, and hysteresis. *Journal of Geophysical Research*, *112*(F3), F03S28. https://doi.org/10.1029/2006jf000664
Shroder, J., Cornwell, K., Oviatt, C., & Lowndes, T. (2016). Landslides, alluvial fans, and dam failure at Red Rock Pass: The outlet of Lake Bonneville. In *Developments in Earth Surface Processes*, (pp. 75–87). Elsevier. https://doi.org/10.1016/b978-0-444-63590-7.00004-4
Smith, D. G. (1994). Glacial lake McConnell: Paleogeography, age, duration, and associated river deltas, Mackenzie River basin, western Canada. *Quaternary Science Reviews*, *13*(9), 829–843. https://doi.org/10.1016/0277-3791(94)90004-3
Sutherland, J. L., Carrivick, J. L., Gandy, N., Shulmeister, J., Quincey, D. J., & Cornford, S. L. (2020). Proglacial lakes control glacier geometry and behavior during recession. *Geophysical Research Letters*, *47*(19), e2020GL088865. https://doi.org/10.1029/2020gl088865
Teller, J. T., & Leverington, D. W. (2004). Glacial Lake Agassiz: A 5000 yr history of change and its relationship to the $\delta^{18}O$ record of Greenland. *GSA Bulletin*, *116*(5–6), 729–742. https://doi.org/10.1130/B25316.1

Wickert, A. D. (2016). Reconstruction of North American drainage basins and river discharge since the Last Glacial Maximum. *Earth Surface Dynamics*, *4*(4), 831–869. https://doi.org/10.5194/esurf-4-831-2016

Wiersma, A., & Renssen, H. (2006). Model–data comparison for the 8.2 ka BP event: Confirmation of a forcing mechanism by catastrophic drainage of Laurentide Lakes. *Quaternary Science Reviews*, *25*(1–2), 63–88. https://doi.org/10.1016/j.quascirev.2005.07.009

References From the Supporting Information

Gowan, E. J., Zhang, X., Khosravi, S., Rovere, A., Stocchi, P., Hughes, A. L. C., et al. (2021). A new global ice sheet reconstruction for the past 80 000 years. *Nature Communications*, *12*(1), 1199. https://doi.org/10.1038/s41467-021-21469-w

Larour, E., Seroussi, H., Adhikari, S., Ivins, E., Caron, L., Morlighem, M., & Schlegel, N. (2019). Slowdown in Antarctic mass loss from solid Earth and sea-level feedbacks. *Science*, *364*(6444), eaav7908. https://doi.org/10.1126/science.aav7908

Latychev, K., Mitrovica, J. X., Tromp, J., Tamisiea, M. E., Komatitsch, D., & Christara, C. C. (2005). Glacial isostatic adjustment on 3-D Earth models: A finite-volume formulation. *Geophysical Journal International*, *161*(2), 421–444. https://doi.org/10.1111/j.1365-246x.2005.02536.x

Peltier, W. R. (1974). The impulse response of a Maxwell Earth. *Reviews of Geophysics*, *12*(4), 649. https://doi.org/10.1029/rg012i004p00649

Waelbroeck, C., Labeyrie, L., Michel, E., Duplessy, J. C., Mcmanus, J. F., Lambeck, K., et al. (2002). Sea-level and deep water temperature changes derived from benthic foraminifera isotopic records. *Quaternary Science Reviews*, *21*(1–3), 295–305. https://doi.org/10.1016/s0277-3791(01)00101-9

Wan, J. X. W., Gomez, N., Latychev, K., & Han, H. K. (2022). Resolving glacial isostatic adjustment (GIA) in response to modern and future ice loss at marine grounding lines in West Antarctica. *The Cryosphere*, *16*(6), 2203–2223. https://doi.org/10.5194/tc-16-2203-2022

Wu, P., & van der Wal, W. (2003). Postglacial sealevels on a spherical, self-gravitating viscoelastic Earth: Effects of lateral viscosity variations in the upper mantle on the inference of viscosity contrasts in the lower mantle. *Earth and Planetary Science Letters*, *211*(1–2), 57–68. https://doi.org/10.1016/s0012-821x(03)00199-7

Zhong, S., Paulson, A., & Wahr, J. (2003). Three-dimensional finite-element modelling of Earth's viscoelastic deformation: Effects of lateral variations in lithospheric thickness. *Geophysical Journal International*, *155*(2), 679–695. https://doi.org/10.1046/j.1365-246x.2003.02084.x